# LANGMUIR

# Templated Assembly of Nanoparticles into Continuous Arrays

Natali Ostrovsky, Guillaume Le Saux, Uri Argaman, I−Te Chen, Timothy Chen, Chih-Hao Chang, Guy Makov, and Mark Schvartzman*

Read Online

ACCESS | 📊 Metrics & More | 📰 Article Recommendations | 🆂🅸 Supporting Information

**ABSTRACT:** The templated assembly of nanoparticles has been limited so far to yield only discontinuous nanoparticle clusters confined within lithographically patterned cavities. Here, we explored the templated assembly of nanoparticles into continuous 2D structures, using lithographically patterned templates with topographical features sized as the assembled nanoparticles. We found that these features act as nucleation centers, whose exact arrangement determines four possible assembly regimes (i) rotated, (ii) disordered, (iii) closely packed, and (iv) unpacked. These regimes produce structures strikingly different from their geometry, orientation, long-range and short-range orders, and packing density. Interestingly, for templates with relatively distant nucleation centers, these four regimes are replaced with three new ones, which produce large monocrystalline domains that are either (i) uniformly rotated, (ii) uniformly aligned, or (iii) nonuniformly rotated relative to the nucleation lattice. We rationalized our experimental data using a mathematical model, which examines all the alignment possibilities between the nucleation centers and the ideal hexagonal assembly. Our finding provides a new approach for the *à la carte* obtainment of various nanoscale structures unachievable by natural self-assembly and opens a route for the fabrication of numerous functional nanodevices and nanosystems that could not be realized so far by the standard bottom-up approach.
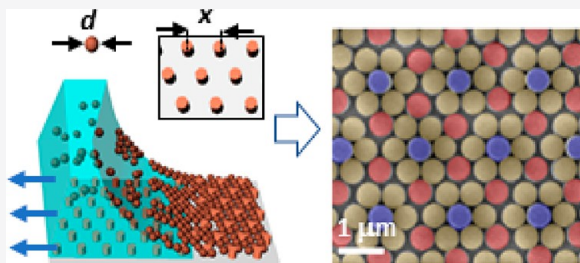
## ■ INTRODUCTION

Bottom-up nanofabrication has long been considered an attractive alternative to traditional top-down nanofabrication. To provide the building blocks for future nanoscale systems, numerous nanomaterials with sizes, shapes, and compositions with atom-level control have been developed in the last two decades with a structural and functional complexity unachievable by standard fabrication approaches.[1−5] On the other hand, controlled assembly of these nanomaterials into desired controlled architectures remains a challenge. Self-assembly naturally organizes variously sized building blocks into ordered architectures,[6] being controlled by van der Waals or capillary forces at the nanometric scale.[7−10] However, self-assembly lacks long-range order and is limited to yield only one specific geometry defined by the thermodynamic minimum of the assembly system. These two major shortcomings of self-assembly have hindered the realization of functional nanoscale structures and systems from the bottom-up.

A powerful approach to overcome the shortcomings of self-assembly is to assemble nanostructures on a template-surface patterned with topographic features with a similar length scale. Such features produce highly localized capillary forces during the assembly, which guide the assembled nanoparticles with a control over long and short-range order and packing density that are unachievable by traditional self-assembly on a nonpatterned substrate.[11] While most broadly studied nanoparticles in the context of capillary templated assembly are

nanospheres,[12] such assembly was also demonstrated on nanosized cylinders,[13−16] cubes,[16,17] prisms,[16] and polyhedral.[18] Applications of templated assembly include, but are not limited to the fabrication of tunable structures for plasmonics,[19] second harmonic generation,[20] surface-enhanced Raman scattering,[21] and light emission.[22] However, state-of-the-art approaches for templated assembly have been mostly based on template patterns containing distinct topographical confinements, that is, pits or grooves, which were designed to trap individual nanoparticles, or their clusters, depending on the confinement size and geometry.[23−31] This templating approach is limited to the production of discontinuous arrays of nanoparticles. On the other hand, many functional nanoscale systems, such as photonic crystals,[32] are based on continuous arrays of nanoparticles, and the ability to control their assembly into templated continuous arrays could unleash the design of such nanosystems from the geometric constraints of self-assembly. Yet, the topographically templated assembly of nanoparticles into continuous structures remains mostly unexplored. Recently, Kadiri et al. reported the assembly of
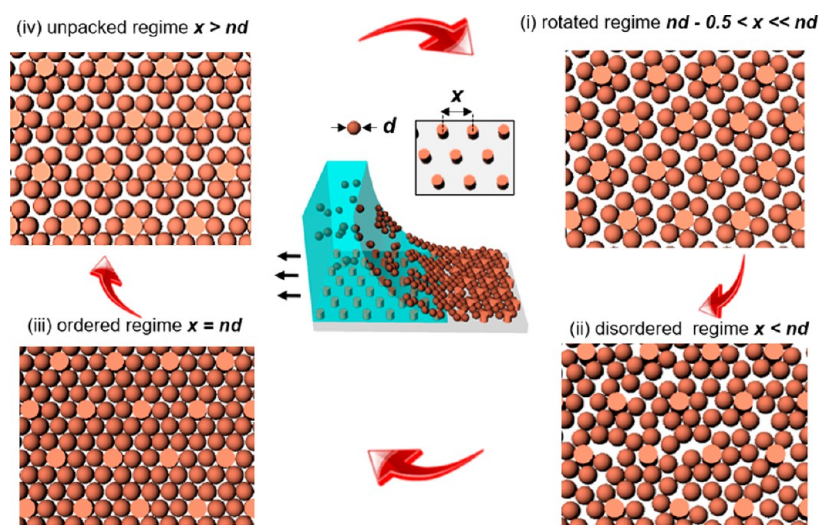
**Figure 1.** Templated assembly of nanoparticles of into continuous films whose structure is determined both by ratio ($n$) between the spacing between the nucleation centers ($x$) and the nanoparticle diameter ($d$). Four different assembly regimes: (i) rotated, (ii) disordered, (iii) closely packed, and (iv) unpacked are schematically shown.

nanospheres onto a pattern of discrete hexagonally arranged nano features spaced as a multiple of the nanosphere diameter, to obtain monocrystalline 2D structures with long-range order.[33] Similarly, Asbahi et al. demonstrated the assembly of nanoparticles onto templates of nanoposts, whose spacing, however, was limited to four nanoparticle diameters, and whose arrangement was limited only to geometries commensurable with closely packed self-assembly.[34] On the other hand, nanoparticle assembly of continuous structures onto templates whose geometry does not fit with the lattice spacing defined by self-assembly is completely unexplored. Even less known is whether templated assembly can produce nonstandard geometries that are normally unachievable by natural self-assembly.

Here, we provide a detailed study of the assembly of nanospheres into architectures deliberately misaligned from an ideal 2D hexagonal crystal. To that end, we designed and fabricated a series of templates patterned with capillary-guiding features spaced equally to or systematically deviating from a multiple of the nanosphere diameter (Figure 1). We characterized the assembled architectures using both long-range and short-range order. We found that the guiding features act as nucleation centers, around which nanospheres are assembled into characteristic unit cells, which are in turn configured into continuous superlattices. Here, the geometry and the orientation of the unit cells and the continuous superlattices are determined by the spacing between the nucleation centers, termed hereafter as $x$. In particular, we found that for templates with hexagonally arranged centers ($x$) spaced around 3 and 5 nanosphere diameters ($d$), the assembly occurs in four different regimes. In the regime ($nd - 0.5 < x \ll nd$) the nanospheres form ordered units that are uniformly rotated relative to the lattice of the nucleation centers. As the spacing increases but is still smaller than an integer of diameters ($x < d$), the assembly enters the second, disordered regime. Then, when the spacing becomes equal to an integer of diameters ($n = d$), the third, ordered regime is obtained, in which the nanospheres and the nucleation centers form together an ideal closely packed hexagonal lattice. Finally, when the spacing further increases ($x > d$), the assembly enters its fourth, unpacked regime, which produces separated

nanosphere clusters, which are aligned to the lattice of the nucleation centers. The existence of the four regimes was confirmed by fast Fourier transform (FFT) analysis of the assembled structures, as well as by their long-range order, short-range order, and density, which all consistently varied among the regimes. Remarkably, for the higher range of spacing between the nucleation, such as $x$ varied around $8d$, the assembly produces large 2D monocrystalline domains. Here, the exact spacing between the nucleation centers determines one of three possible assembly regimes, by which the crystalline domains are either (i) uniformly rotated, (ii) uniformly aligned, or (iii) nonuniformly rotated relative to the lattice of the nucleation centers. We rationalized our experimental findings using a simple geometrical model that treats the nucleation centers as localized perturbations in the closely packed hexagonal self-assembly of nanoparticles, whose spacing defines whether the obtained assembly structure will be ordered or disordered, and which spatial orientation it will have in the first scenario. Our findings provide new insight into nanoscale self-assembly, and pave the route to numerous nanoscale systems with unparalleled structural control and complexity, which are fabricated by combined top-town and bottom-up approaches.

## 1. EXPERIMENTAL SECTION

The templates were produced by patterning silicon substrates by electron beam lithography (Raith eLine), using an organic negative tone resist (SU8−2002), which was diluted in solvent (1:1 v/v), spin coated at 3500 rpm for 30 s to obtain a film with a thickness of 600 nm, and baked on hot-plate at 95 °C for 1 min. After exposure, the resist was developed for 1 min in a commercial developer (PGMEA), rinsed with isopropanol and dried with under a stream of nitrogen. A dispersion of 500 nm polystyrene nanoparticle (2.6% solids, PolyScience) was concentrated to 8% by centrifugation, followed rinsing with water, and adding an appropriate amount of water and ethanol (2:1 v/v). The nanoparticle dispersion was then spin-coated on the templates with a speed of 1000 rpm for 1.5 min. The spin-coating of the nanoparticle dispersion was performed in a clean room environment with a controlled temperature of 25 °C and a relative humidity of 40%. With these parameters, the highest coating density in self-assembly was achieved. The assembled structures were inspected by scanning electron microscopy (SEM) (FEI Verios
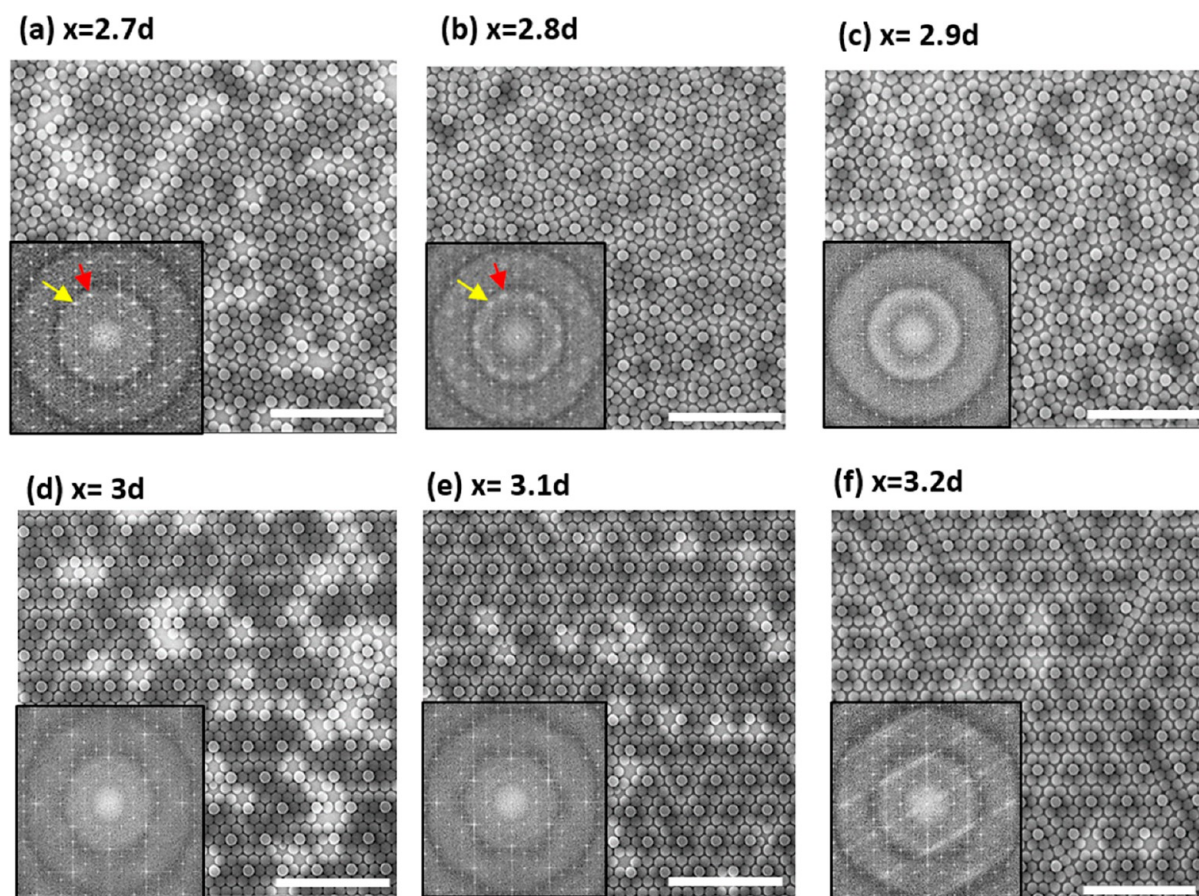
**Figure 2.** Assembly of nanoparticles onto templates patterned with nucleation centers for *x* varied around *3d*. FTT patterns are also shown (inset). Scale bars: 5 $\mu$m. Insets: FFT patterns.

460L). The images were analyzed using both the ImageJ imaging software as well as MATLAB to obtain 2D FFT and 1D FFT.

## RESULTS AND DISCUSSION

Templates for the controlled assembly of nanospheres consisted of hexagonally arranged nucleation centers, which were patterned by negative tone electron beam lithography on Si substrates using an organic resist. Notably, the centers were based on the patterned resist, that is, no further pattern transfer to Si was needed after the lithographic step. The height and diameter of the nucleation centers were kept equal to the diameter of the assembled nanospheres (500 nm). This was achieved by tightly controlling the resist thickness and exposure dose. The arrays of nucleation centers were designed with spacings *x,* whose values were systematically varied. An aqueous monodisperse suspension of polystyrene nanospheres was casted onto the fabricated templates by spin-coating, and the resulting 2D structures were inspected by Scanning Electron Microscopy (SEM).

Figure 2a−e show typical assembly patterns formed on the templates in which the center-to-center spacing between the nucleation centers was systematically varied from *2.7d* to *3.2d*. Although the increments between the probed spacing values were relatively small, these templates yielded assembled structures that were strikingly different. At a glance, templates with spacings smaller than *3d* seemingly produced disordered structures (Figure 2a−c), while templates with spacings of *3d* and higher appeared to produce ordered structures (Figure 2d−f). Fast Fourier Transform (FFT) algorithm was used to

quantitatively assess the degree of order of the obtained structures. The resulting reciprocal lattices are shown in the insets of the SEM images. In sharp contrast to our first assessment, the FFT images revealed that the templates with *x* < 3d were in fact not completely disordered. First, at *x = 2.7d*, sharp nodes on these reciprocal lattices correspond to the nucleation centers, whose precise hexagonal periodicity was encoded by electron beam patterning. Additional sharp nodes correspond to the ordered location of the assembled nanoparticles, which has two visible kinked conformations rotated relative to the nucleation centers, as shown in Supporting Information (SI) Figure S1a, as well as by red and yellow arrows in the reciprocal pattern of Figure 2a and SI Figure S1b. As the spacing increases (x = *2.8d*), the two kinked conformations are still visible (SI Figure S2a), but the nodes become blurry in the FFT image (Figure 2b and SI Figure S2b), indicating that the assembled structure loses crystallinity. We presume that this behavior stems from a slight increase in the degree of freedom of the spheres, and therefore their position can vary relative to the kinked conformations observed in *2.7d*. Interestingly here, and contrary to the case of *2.7d*, we do not observe large crystalline domains with one direction only. This also explains the nodes being less sharp, since large domains equate to long-range order. However, the two directions are still visible, as shown by the two pairs of dots in Figure 2b, and it therefore appears like the two kinked conformations coexist down to the scale of neighboring nucleation posts. Finally, for *2.9d*, crystallinity appears to be totally lost with the hexagonal patterns of the nucleation post
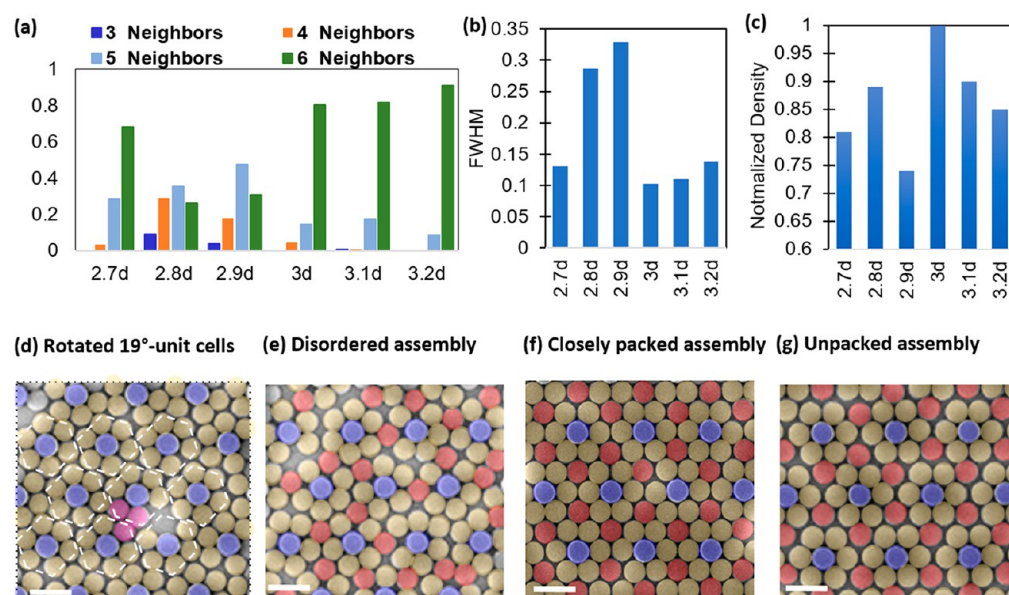
**Figure 3.** Assembly analysis for the templates with *x* varied around *3d*. (a) The fraction of nucleation centers with the different number of neighboring nanoparticles vs the spacing between the nucleation centers (b) fwhm of spots on the reciprocal pattern vs the spacing between the nucleation centers. (c) The density of the nanospheres normalized to the maximal possible density that can be obtained at the perfect self-assembly to the closely packed hexagonal geometry. (d−g) Four different regimes of the templates assembly for *x* varied around *3d*. Scale bar: 1 *μm*.

solely remaining. For periodicities of *3d* and higher, the kinked conformations completely disappear and the nanospheres align perfectly with the nucleation centers. On the other hand, in the FFT pattern of the *3.2d* periodicity, the node relative to the nanospheres appears smeared with an angle of 30° (Figure 2f). This smearing comes from variations in interparticle distances at grain boundaries due to the larger degree of freedom given by the *3.2d* spacing. Interestingly the smears are only visible in one direction.

We further quantified the crystallinity of the formed 2D structures in three terms: short-range order, long-range order, and total surface density. First, we characterized the short-range order by means of the number of nanospheres adjacent to each nucleation center, henceforth referred to as nearest neighbors. This is accomplished using an image processing algorithm, where the centers of each particle/template structure are calculated using a correlation kernel and compared to identify the relative distances to the nearest neighbor.[35] Theoretically, each nucleation center can have up to six nearest neighbors for a hexagonal close packed lattice. Thus, we defined the percentage of nucleation centers having six nearest neighbors as the figure of merit for short-range order. Figure 3a shows the distribution of the numbers of nearest neighbors vs the spacing between the centers. It can be seen that for the lowest spacing of *2.7d*, only around 70% of the nucleation centers have six nearest neighbors. This percentage further decreases with increasing in spacing, reaching a minimum of ∼30% for *2.8d* and *2.9d*. Then, this percentage abruptly rises at *3.0d*, and continues to increase, until it reaches more than 90% for the highest probed periodicity of *3.2d*.

Next, we quantified the long-range order of the assembled structures using their reciprocal FFT patterns. It should be noted that whereas the spot position in the reciprocal lattice informs about the size of the unit cells, the shape and size of the spots are affected by the long-range order and arrangement of the unit cells. To quantitatively assess how long-range order is affected by the spacing between the nucleation centers, we plotted cross-section profiles of the nodes in each case and measured their full-width at half-maximum (fwhm) values (Figure 3b) as well as their normalized intensity (Figure 3c) (see SI Figure S3a,b). In this case, both the fwhm and their normalized intensity allow to quantify the degree of deviation from the ideal packing scenario. Interestingly, fwhm vs *x* shows a trend similar to that obtained for the short-range order: the spots gradually broaden with the low spacings of *2.7d* to *2.9d*, indicating a systematic decrease in the long-range order. Then fwhm abruptly falls at *3.0d* to the value that corresponds to the highest obtained long-range order, and finally slowly increases for higher periodicities. Lastly, the surface density of the nanospheres shows no clear trend for the low range of periodicities, with variations of ±1% that can be attributed to random fluctuations. However, the density abruptly increases at *3.0d*, confirming that this periodicity is a "breakpoint" between different states of assembly (Figure 3c).

To interpret the data of Figure 3a−c, a more detailed analysis of the obtained structures was performed. This analysis revealed four different regimes of assembly, depending on the range of the spacing between the nucleation centers. In the first regime, which occurs for the spacings of *2.7d* and *2.8d*, and is shown in detail in Figure 3d, most of the nucleation centers (false-colored in blue) are surrounded by closely packed six nanospheres (false-colored in yellow). Each center and six nanospheres form a hexagonal unit cell. The unit cells themselves are arranged in a hexagonal lattice according to the arrangement of the nucleation centers. As previously observed, the unit cells are rotated by an angle of about 19° to the horizontal base vector of the lattice of the nucleation centers. Remarkably, the assembled pattern contains large domains, in which this rotation is either clockwise or counterclockwise (SI Figure S1a). These two symmetrical rotations produce two rotated sets of spots in the reciprocal pattern marked by red and yellow arrows in FFT. Since both rotations are symmetrical, we will henceforth consider one
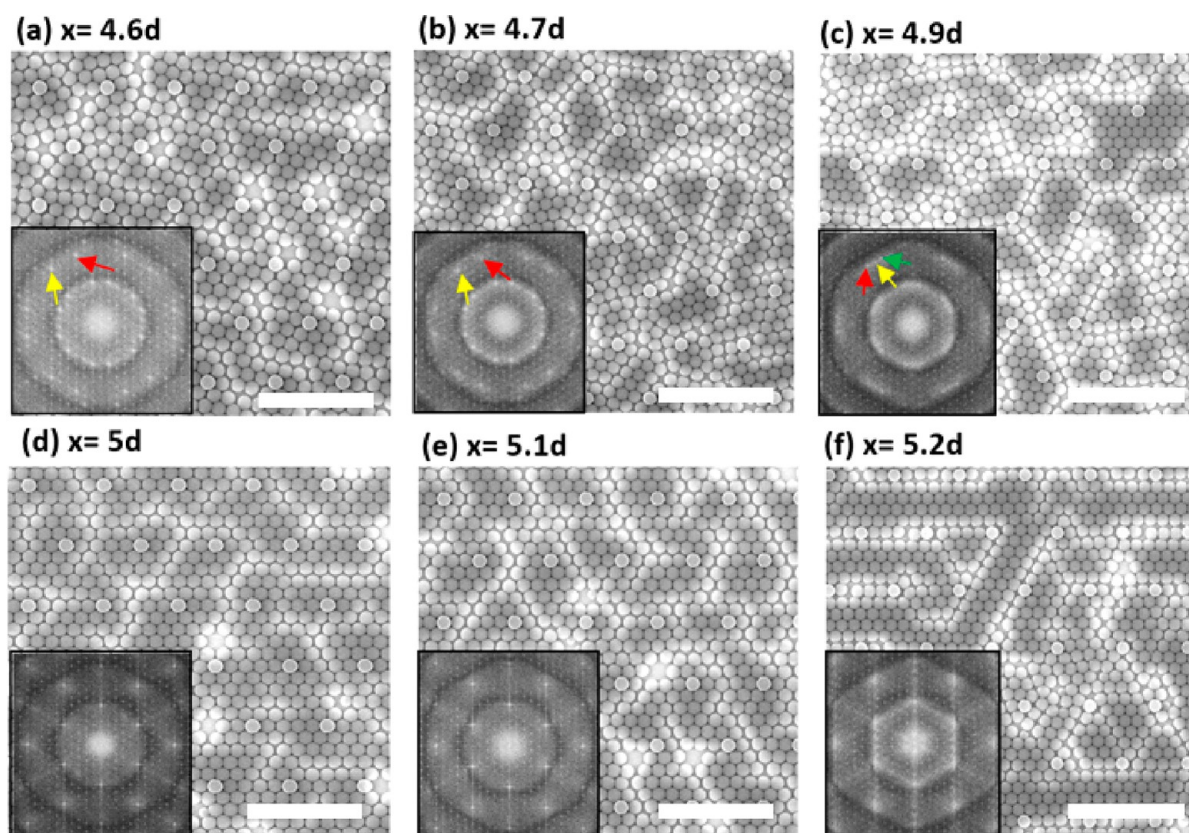
**Figure 4.** Assembly of nanoparticles onto templates patterned with nucleation centers whose spacing was varied around *5d*. Scale bars: 5 *μ*m. Insets: FFT patterns.

angle only. Here, adjacent nanospheres from different unit cells are juxtaposed and assembled in triads to form a nearly perfect equilateral triangle (false-colored in pink in Figure 3d). We thus conclude, that for a sufficiently small spacing between the nucleation centers, the capillary forces formed by the dried solvent yield the closest packing possible, both between the nanospheres of the same unit cell, as well as between the nanospheres in adjacent cells. Furthermore, in this conformation, minimizing the distance between the adjacent nanospheres in two different unit cells induces the observed uniform rotation angles. On the other hand, increasing the spacing from *2.7d* to *2.8d*, gives more leeway for the triad which in turn explains the increase in fwhm (Figure 3b). However, this increased leeway has a second, more profound impact. The low freedom of movement in the case of *2.7d*, enables the formation of large stable domains and thus long-range order. Conversely, the subtle increase to *2.8d* disrupts this long-range stabilization and therefore induces the formation of small domains, sometimes down to a single unit cell.

As the spacing between the nucleation increases to *2.9d*, the arrangement of the assembled nanospheres becomes highly disordered (Figure 3e). Here, the vacancy between the formed unit cells is large enough to include additional "interstitial" nanospheres (false-colored in red). Yet this vacancy is too small to allow a uniform and symmetrical arrangement of these interstitial nanospheres, which are thus positioned randomly. The random interstitial nanospheres cause the random rotation of the hexagonal unit cells around the nucleation centers, thereby reducing the long-range order. This explains the spot broadening in the reciprocal lattices shown in Figures

2b−c, which is also quantified in Figure 3b. Furthermore, many interstitial nanospheres distort the ordered hexagonal structure of the unit cells by pushing the neighboring nanospheres out of the unit cells, and thereby reduce the short-range order of the assembly for *2.9d* spacing, as reflected in Figure 3a.

We next investigated the *3.0d* spacing, which is a critical "breakpoint" at which two nanospheres fit exactly between two nucleation centers. This fitting enables a closely packed hexagonal assembly, at which all the hexagonal unit cells are now oriented uniformly and aligned with the lattice of the nucleation centers (Figure 3f). In addition, the interstitial nanospheres are now arranged symmetrically, and form, together with the hexagonal unit cells, a perfect hexagonal 2D lattice. The high order of this lattice is reflected in the relatively high proportion of nucleation centers with six nearest neighbors, approximately 80%. The other nucleation centers are surrounded by five or four nanospheres, which can be attributed to random defects. Furthermore, the obtained perfect hexagonal lattice has a relatively long-range order, as reflected by the sharp node in the reciprocal lattice (Figure 2f), and, as a consequence, the smallest fwhm among the probed spacings (Figure 3b). Finally, the transfer from a disordered regime to a closely packed ordered assembly explains the abrupt increase in the surface density of nanospheres, which has also the highest value among the obtained structures (Figure 3c).

When the spacing between the nucleation centers further increases above *3d*, the assembly enters a fourth, unpacked regime (Figure 3g). Interestingly, here the hexagonal unit cells are still uniformly oriented parallel to the lattice formed by the
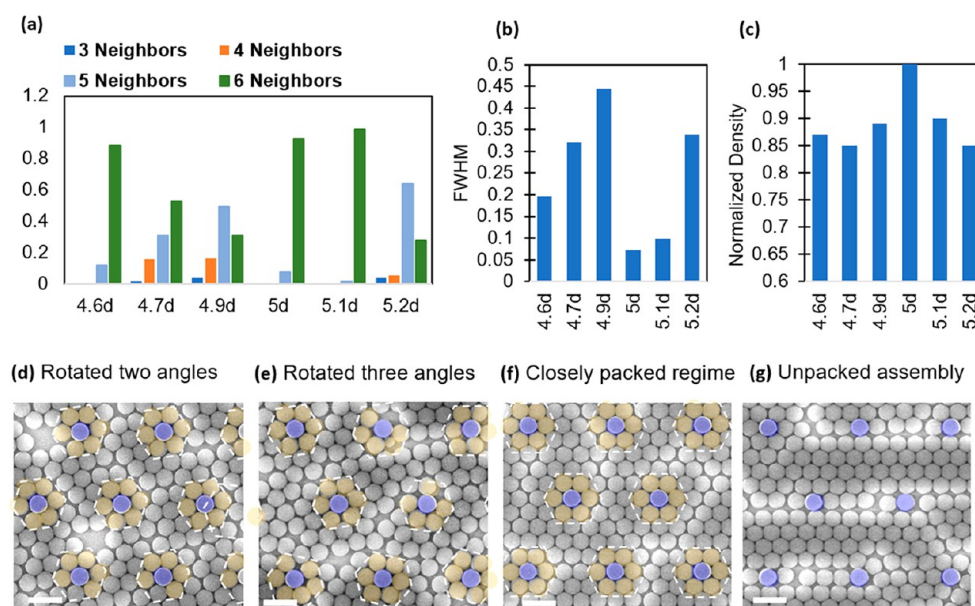
**Figure 5.** Assembly analysis for the templates with *x* varied around *5d*. (a) Fraction of nucleation centers with different numbers of neighboring nanoparticles vs the spacing between the nucleation centers (b) fwhm of nodes on the reciprocal pattern vs the spacing between the nucleation centers. (c) Density of nanospheres normalized to the maximal possible density obtained with closely packed hexagonal geometry. (d−g) Four different regimes of the templates assembly for *x* varied around *5d*. Scale bar: 1 *μ*m.

nucleation centers, as in the previous, closely packed regime, even though the relatively large spacing between the nucleation centers allows, in principle, for their rotation. Also, the position of interstitial nanospheres is not random. Each interstitial nanosphere is surrounded by six neighboring nanospheres, and in most cases, the interstitial nanospheres stick to one or two "upper" nanospheres located upstream from the flow of the drying meniscus of the nanoparticle dispersion. Together, the hexagonal unit cells and the adjacent interstitial nanospheres form an ordered structure with an overall nanosphere density lower than that of the closely packed assembly (Figure 3c).

The above-described assembly regimes were observed for templates with relatively dense nucleation centers. Naturally, we next tested whether a similar assembly behavior can be obtained for nucleation centers arranged with lower densities. Figure 4a−f shows assembly images and the corresponding FFT patterns obtained on the templates, in which the nucleation centers were varied around *5d*. Similar to the previously described assembly for *3d*, here we can qualitatively observe a gradual shift from a less ordered to a more ordered assembly with the increase in the spacing between the nucleation centers. In addition, we also observe the two kinked conformations schematically marked by yellow and red arrows in the FFT patterns for *4.6d* (SI Figure S4a,b) and *4.7d* (SI Figure S5a,b). In these two instances and similar to the *3d* case, a slight increase in the spacing induces more leeway which is transcribed in a broadening of the nodes in the FFT patterns. However, and opposite to the *3d* case, long-range order seems less affected as relatively large domains are visible for both *4.6d* and *4.7d* cases. On the other hand, *4.9d*, Figure 4a and SI Figure S6a, does not behave like its *2.9d* counterpart. Whereas the *2.9d* was fully disordered, here, a third position of equilibrium is possible as seen from the three nodes in Figure 3c (marked in red, yellow, and green arrows). This is especially visible in the second harmonic shown in the inset of Figure 4c and in SI Figure S6b. Here, in addition to the two kinked conformations on either side of the normal, which were

previously observed, a third confirmation, aligned with the pattern of the nucleation points is visible. For periodicities of *5d* and upward, the regime of assembly appears similar to the *3d* case, with nanosphere solely aligned with the nucleation post and gradual increase in unpacked assembly. Similar to the *3.2d* case (Figure 2f), we observe smears in FFT for the *5d*, *5.1d*, and *5.2d* cases (Figure 4d−f). As previously mentioned, this smearing comes from variations in interparticle distances at grain boundaries which is due to the larger degree of freedom. However, in contrast to *x* = *3.2d* for which the smear in the FFT pattern was unidirectional, we observe here that the smears align with the three main directions of the hexagonal lattice. This is also visible in the SEM images with the alignment of the grain boundaries. In addition, grain size appears to increase from *5d* to *5.2d*. More work on deciphering the reasons underlying this trend with be performed in follow up work.

We also quantified the crystallinity of the formed 2D structures in terms of short-range order, long-range order, and total surface density. Assembly on the template with the shortest spacing (*x* = 4.6d) yielded a relatively high percentage of completely hexagonal unit cells, in which each nucleation center is surrounded by 6 nanospheres (Figure 5a). This number then decreases for *4.7d* and *4.9d* and, as observed on the *3d* templates, the *5d* periodicity acts as a breaking point where the percentage of 6 nearest neighbors jumps once again. This increase in short-range order is also visible in the long-range as reflected by a sharpening of the nodes in the FFT pattern (Figure 4d inset) and the smallest fwhm (Figure 5b) as well as a markedly high packing density (Figure 5c). For the templates larger than *5d*, the previous trend is recovered where, in addition to packing density, both long-range and short-range orders decrease (Figure 5a−c).

Detailed analysis of the assembly on the templates with ∼ *5d* periodicity reveals the existence of four regimes governing the templated nanoparticle assembly. These are (i) rotational with two conformations in the case of *4.6d* and *4.7d* (Figure 5d),
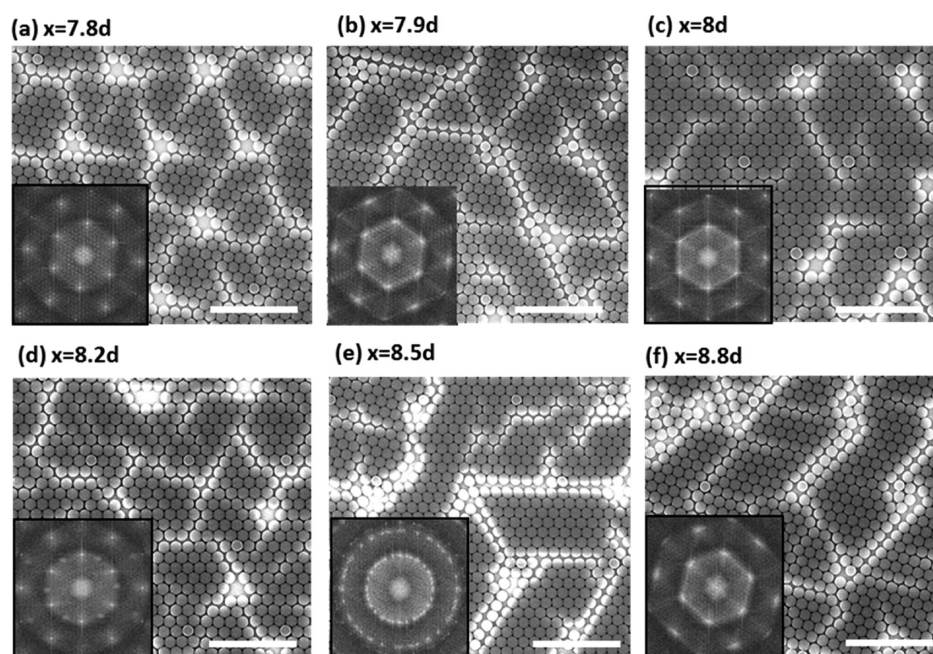
**Figure 6.** Assembly of nanoparticles onto templates patterned with nucleation centers whose spacing was varied around $8d$. Scale bars: 4 $\mu$m. Insets: FFT patterns.

(ii) rotational with three conformations for $4.9d$ (Figure 5e), (iii) closely packed regime for $5d$ and $5.1d$ (Figure 5f), (iv) unpacked assembly for $5.2d$ (Figure 5g). Notably, the $3d$ and $5d$ templates share the regime with two kinked conformations, however, unlike the 2.9d case which was fully disordered, the larger periodicity allowed for the formation of a supplementary ordered regime with three conformations. Then, as in the $3d$ case, assembly on the $5d$ template represents a breaking point. Furthermore, when the spacing is slightly above the multiple of diameters, ($5.1d$ in Figure 4e), the closely packed regime is maintained. Yet, when the spacing is further increased to $5.2d$, the assembly enters a fourth, "unpacked" regime (Figure 4f), which is, however, strikingly different from that obtained on the templates with $x$ varied around $3d$. In particular, while the unpacked assembly for $x > 3d$ resulted in uniform and highly organized crystalline clusters, each of which contains a nucleation center with six nearest neighbors, here the nanospheres do not necessarily organize around the prepatterned nucleation centers. Instead, the nanospheres are assembled in relatively large crystalline domains with relatively random sizes and shapes. These clusters are separated by arbitrary grain boundaries, many of which interface the nucleation centers. This relative disorder of the fourth regime is reflected by a low percentage of the centers with six neighboring nanospheres (Figure 5a), as well as by the broadened nodes on the reciprocal lattice (Figure 4f inset and 5b). Importantly, and contrary to the $3.2d$ case (Figure 2f), the smears are visible in all three directions of the hexagonal lattice. This, along with the appearance of a rotational regime with three degrees of freedom (Figure 4c) suggests that increasing periodicity gives further latitude in the way the nanospheres assemble on a template.

It should be noted that despite obvious similarities between the assemblies of $3d$ and $5d$ cases, the regimes are more pronounced for the $3d$ case. To check whether these regimes also exist for a higher range of spacings between the nucleation centers, we assembled nanospheres onto templates in which the nucleation centers were variably spaced around $8d$ (Figure 6). The qualitative analysis did not reveal drastic differences in the obtained 2D structures for the probed variations in spacing. Indeed, all the templates yielded polycrystalline structures consisting of large monocrystalline domains separated by random grain boundaries. Furthermore, these monocrystalline domains are not formed around individual nucleation centers, as observed for the previously described templates. Instead, the nucleation centers are mostly located at the boundaries between the crystalline domains, and they seem to disrupt the formation of the crystalline structures instead of driving their assembly. Yet, at least one geometrical parameter of the assembled structure is still determined by the spacing between the nucleation centers, which is the tilt angle of the crystalline domains with regards to the lattice of the nucleation centers.

A more detailed analysis of the patterns in Figure 6a,b reveals that for the templates with $x < 8d$, the crystalline domains are uniformly rotated by ~6.5° compared to the axis of the lattice formed by the nucleation centers. This rotation defines the first assembly regime, which we termed as "uniformly rotated assembly". Remarkably, for this periodicity, the rotational regime with two tilt angles is not maintained anymore. At $x = 8d$ (Figure 6c), the crystals align with the nucleation lattice. This regime, which was also observed for $3d$ and $5d$ is defined as "aligned assembly". However, for this periodicity, the larger nodes in the FFT pattern indicate a lesser degree of crystallinity. Above $8d$, a whole new mechanism appears to take place. Even though relatively large domains of hexagonally packed nanospheres exist, the FFT suggests that although the nanospheres assemble with varying rotation angles relative to the nucleation centers, the sharpness of the nodes indicates that these tilt angles have in fact discrete values. As the spacing increases from $8.2d$ to $8.5d$, the number of discrete values increases from 3 rotation angles (Figure 6d) to a large amount of rotation angles, but not all of them, since continuous and diffuse rings are not observed (Figure 6e inset). Further increase of $x$ to $8.8d$ yields an
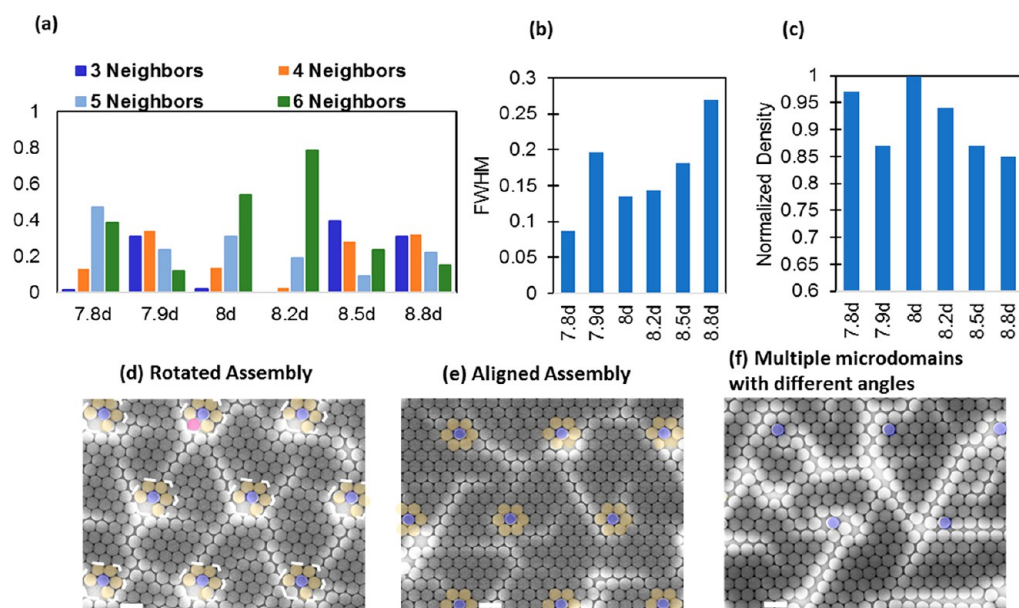
**Figure 7.** Assembly analysis for the templates with x varied around *8d*. (a) The fraction of nucleation centers with the different number of neighboring nanoparticles vs the spacing between the nucleation centers (b) fwhm of spots on the reciprocal pattern vs the spacing between the nucleation centers. (c) the density of the nanospheres normalized to the maximal possible density that can be obtained at the perfect self-assembly to the closely packed hexagonal geometry. (d−e) Different regimes of the templates assembly for *x* varied around *8d*. Scale bar: 1 μm.

assembled structure almost identical to that of *7.8d* and *7.9d*. Here, the major tilt angle around 6.5° is also present, but the blurriness of the nodes is indicative of a wider distribution of the angles. This is indicative of a higher degree of freedom in the assembly of the nanospheres (Figure 6f).

Short-range order, long-range order, and total surface density were also quantified for the various templates around the *8d* periodicity. Analysis of the nearest neighbors did not reveal a specific trend with relative spacing (Figure 7a). This is in good agreement with the observation that the nucleation centers are mostly located at the boundaries between the crystalline domains. Remarkably, the other two figures of merit for the assembly—fwhm of the spots in reciprocal lattices and nanosphere surface density—do not show any pronounced difference or trend between the various spacings (Figure 7c,d). This is especially true for *8d* whose values do not stand clear of the other conditions. This sharply contrasts with the *3d* and *5d* periodicities which had the highest long-range, short-range order and packing density. This suggests that as periodicity increases, more defects can be observed and the level of control over assembly is gradually lost. Nevertheless, within this periodicity, a tight control over the assembly is still possible, since three distinct regimes are observed. The first regime is uniformly rotated assembly seen for the *7.8d*, *7.9d*, *8.8d* templates. In the regime, we observed the same rotation angle relative to the nucleation lattice, but also observed a decrease in order as spacing increases. The substrate with the *8d* periodicity is under the second regime which corresponds to the perfect alignment also observed for the *3d* and *5d* templates. Interestingly, many nucleation centers have one, uniformly located and oriented vacancy of nanosphere, as clearly seen in Figure 6a. The origin of this uniformity is a subject of future studies, but we now speculate that it possibly stems from the flow direction of the meniscus of the nanosphere containing dispersion during the spin coating. Finally, *8.5d* represents the third regime, at which multiple microdomains with different angles coexist. Notably, *8.2d* can

be considered as a transitional stage between the second and third regimes. Two interesting features must be noticed regarding this assembly. First, although the third regime allows multiple angles of rotation, these angles are not random, but seem to have very well-defined values. Second, the *7.8d* and *7.9d* templates produce strikingly the same assembly as the *8.8d* template. This confirms that the behavior of the assembly is cyclical in regards to the periodicity of the nucleation centers.

Self-assembly of nanoparticles onto a template with distinct topographic features can be analyzed by modeling the accumulation of the particles at the meniscus front, and their movement within the features driven by localized capillary forces during the meniscus drying. However, for the geometry described here, in which most of the area is covered by the assembling nanoparticles, and the topographic features (e.g., nucleation centers) are sparse, such a kinetic analysis might be very complex. Instead, we applied a simple geometric analysis of the obtained assembly patterns. It is well-known that for spherical particles with isotropic force fields in 2D, the stable close-packed structure is a hexagonal lattice.[36] Thus, the lattice of nucleation centers can either align with the perfect hexagonal lattice of the nanoparticles, and thus assist its formation, or misalign from the lattice, and thereby produce localized perturbations to its order. The first, idealized scenario, schematically shown in Figure 8a, represents the case of the *3d* template. Here, all the possible positionings of the nucleation centers exactly in alignment with the ideal hexagonal lattice of the nanoparticles are shown. One single nucleation center (colored in gray) can have three groups of neighboring nucleation centers consistent with a hexagonal lattice of the nanoparticles. The first group, which is colored in green, is quite obvious, and consists of nucleation centers arranged parallel to the lattice of the nanospheres. For this group of centers, the separation between the two neighboring nucleation centers is equal to an integer of diameters. The two other groups, which are symmetrical and colored in red and
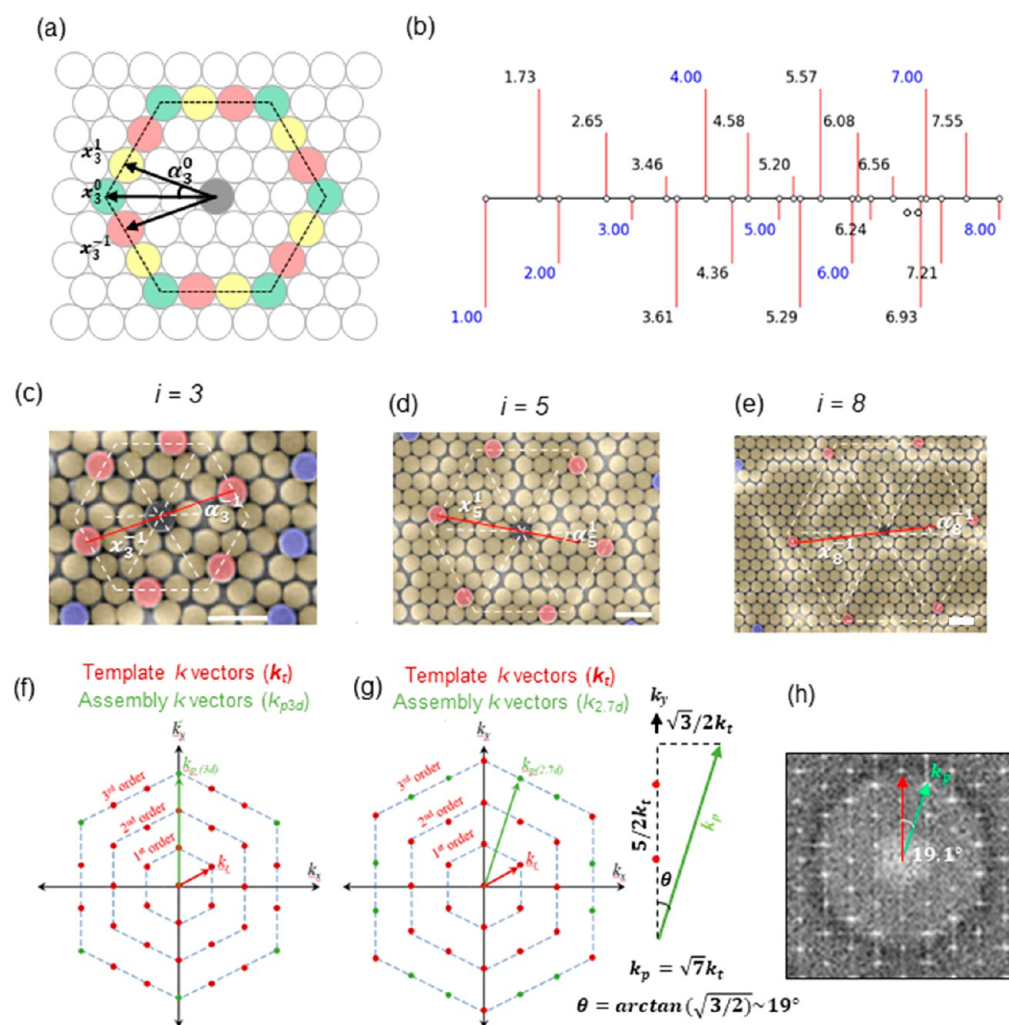
**Figure 8.** (a) Illustration of an ideal hexagonal lattice with three possible arrangements of nucleation centers for 3d case. (b): All distances in the range $d = 1-8$ for the nucleation centers in which a close-packed structure can be assembled. (c)−(e) Patterns of templated assembly rotated by $\alpha_3^0$, $\alpha_5^1$, and $\alpha_8^{-2}$ (see text for definition). The assembled nanoparticles present an ordered hexagonal lattice, whereas the nucleation centers appear as the part of lattice, and are positioned on the edges of a hexagonal cell. (f) Template and particle vectors on the frequency domain for $x = 3d$. (g) Template and particle vectors on the frequency domain for $x = 2.7d$. (f) experimental FFT pattern for $x = 2.7d$, with the measured angle between two adjacent $k_p$ vectors.

yellow, consist of nucleation centers that also align with the hexagonal lattice, but are rotated relative to the original lattice, and are spaced from the gray nucleation center by a noninteger number of diameters.

This approach can be generalized for all possible spacings between the nucleation centers. For this purpose, we first determine hexagonal shells formed by the nanospheres of diameter $d$ that surround a nucleation center at the origin colored in the gray center (Figure 8a). Each shell has an index $i$ determined by the center-to-center distance (in the units of the sphere diameter) from the center to a sphere at the shell corner. Each shell consists of $i$ hexagonal "sextets" of possible nucleation centers, among which one sextet of the centers positioned in the shell corner belongs to the first, aligned group, and other sextets belong to the rotated groups. In this way, the shell with the smallest index $i = 1$ consists of the six spheres closest to the nucleation center at the origin (gray in Figure 8a) that are aligned to the hexagonal lattice; the shell with the index $i = 2$ consists of 12 possible nucleation centers forming two sextets, one which is aligned with the nanoparticle lattice and another rotated. The shell with the index $i = 3$

consists of 18 possible nucleation centers forming three sextets, shown in different colors in Figure 8a: one aligned sexted (green), and two symmetrically rotated sextets (red and yellow). Next, the sextets in each shell have rotation indexes $j$, where $-i/2 \leq j \leq i/2$ for even $i$, $-(I-1)/2 \leq j \leq (I-1)/2$ for odd $i$. The zero value of $j$ corresponds to the aligned sextet in each shell. Other, higher values of $j$ correspond each to rotated sextets, while positive and negative $j$ values correspond to the clockwise and counterclockwise rotations, respectively. For the shells with $i = 1$, the only possible value for $j$ is 0. For the shell with $i = 2$, $j = 0$ corresponds to the aligned sextet, and $j = \pm 1$ corresponds to one rotated sextet. For the shell with $i = 3$, $j = 0$ corresponds to the aligned sexted (colored in green), $j = -1$ corresponds to the counterclockwise (red) rotated sextet, and $j = 1$ corresponds to the clockwise (yellow) rotated sextet. A similar hierarchy of sextets takes place for the shells with higher values of $i$. It should be noted that for an even $i$, $j = -i/2$, and $j = i/2$ correspond to the same sextet. Finally, the center-to-center distances from the nucleation center at the origin (gray) to possible centers can be calculated from the cosine theorem and is equal to

$$x_i^j = d\sqrt{i^2 + j^2 - 2i|j|\cos(60°)} = d\sqrt{i^2 + j^2 - i|j|} \qquad (1)$$

For the centers belonging to the aligned (green) sexted ($j$ = 0), these distances are simply equal to an integer number of diameters, $d$, as mentioned above. As to the distances to the nucleation centers in the rotated sextets, they gradually decrease as $j$ increases. All the resulting permitted nearest neighbor distances between $d$ to $8d$, which are relevant for this study, are presented in Figure 8b. Similarly, the rotation angles can be calculated from using the cosine theorem,

$$\alpha_i^j = \arccos((i^2 + (x_i^j/d)^2 - j^2)d/2ix_i^j) \qquad (2)$$

The analysis of the first set of experiments for which center-to-center distance between the nucleation centers was varied around $3d$ was performed. The experimental results show a relatively high order for the spacing between the nucleation centers of $2.7d$. This order is well mirrored in the model, which predicts a lattice of nucleation centers spaced by $2.66d$ for $i$ = 3 and $j$ = ±1, which ideally align with the perfect hexagonal lattice. Yet, these centers belong to a rotated (red or yellow) group, which explains why the assembled nanospheres formed uniformly rotated units around each nucleation center. To further emphasize the fit between the experimental results and the model, we rotated Figure 3d by 19.1°, which corresponds to $\alpha_3^{\pm1}$. The rotated image is shown in Figure 8c. Now, the nanospheres that were previously attributed to the "rotated assembly regime" seem to form a nearly perfect hexagonal lattice, while the nucleation centers are arranged according to the ideal position defined by $i$ = 3 and $j$ = ±1 indexes. The increase in the distance between the nucleation centers naturally leads to their misalignment from the ideal hexagonal lattice formed by the nanospheres until it reaches an integer multiple of radius, $3d$ in this case. Here, the nucleation centers are located at the corners of the hexagonal shell, and the entire system reaches the highest order. Further increase in the spacing causes a misalignment of the nucleation centers from the hexagonal lattice again, resulting in the loss of order.

The pattern of transformation between ordered and disordered assemblies caused by alternating alignments and misalignments of the nucleation centers to the hexagonal lattice is repeated for the shells with a higher index. Experimental variation of the distance between the nucleation center around $5d$ revealed a highly ordered assembly pattern for $4.6d$, which was attributed to the rotated regime. This distance is very close to $4.56d$, which is predicted by the geometrical model to provide an alignment of the nucleation centers, with the indexes of $i$ = 5 and $j$ = 1. Rotating Figure 5d, which represents the rotating regime, by 10.9° that corresponds to $\alpha_5^{\pm1}$, reveals a nearly perfect hexagonal lattice of the assembled nanospheres, with the nucleation centers located on the edges of the hexagonal shell with $i$ = 5 (Figure 8d). Again, increasing the spacing between the nucleation centers causes their misalignment from the ideal lattice until it reaches the integer multiple of the nanosphere diameters, $5d$, and the order is restored, this time with the nucleation centers located at the corners of the shell. It should be noted that according to the model, the next spacing for which the nucleation centers align with the hexagonal lattice is $5.2d$. However, the experimental results for $5.2d$ shown in Figure 4f reveal polycrystalline lattice, in which some of the crystalline domains are rotated by an angle predicted by the model, while others are still aligned to the lattice of nucleation centers. This

nonuniform orientation of different domains is the main factor for the relative disorder of this pattern.

Finally, the effect of alignment between the nucleation centers and hexagonal lattice on the order of the formed assembly can be analyzed for $i$ = 8. Here, the minimal experimentally probed distance between the patterned nucleation centers was $7.8d$, which is higher than $x_8^{\pm1}$ = $7.55d$. Still, rotating the corresponding assembly pattern by ~6.5°, which is $\alpha_8^{\pm1}$, reveals a nearly perfect hexagonal pattern with the nucleation centers positioned next to the corners of the hexagonal shell (Figure 8e). Again, the order decreases until the spacing reaches $8d$, and the lattice of nucleation centers becomes parallel to that of the assembled nanoparticles. Further increase in x results in multiple crystalline domains that are differently oriented until x reaches $8.8d$. This spacing corresponds to the spacing between nucleation centers positioned next on the edges of the shell with the index $i$ = 9, and thus an ordered rotated structure is obtained again.

Remarkably, the assembly analysis described above was done in the spatial domain. Alternatively, same results can be obtained from the analysis in the reciprocal domain, which can sometimes be more intuitive, and well matches the obtained FFT patterns. In particular, this analysis allows simple calculation of the optimal template period for the off integer assemblies (like $x$ = 2.7d for example), and predicts the rotation angles that align) very well with the observed assembly. The schematic in Figure 8(f−g) illustrates the two cases of $x$ = 3d and $x$ = 2.7d. In the former case, the $k$ vectors of the template ($k_t = 2\pi/x = 2\pi/3$d) are shown in red, and they correspond to the peaks shown in the FFT. Since the particles are nominally 3 times smaller, the k vector for particle assembly would be $k_p = 2\pi/d$, that is, having exactly three times larger magnitude than $k_t$. Thus, here $k_t$ and $k_p$ vectors should align on the six main third order peaks, exactly as obtained in the experimental FFT pattern (Figure 2a inset). The other third order peaks (and also second order peaks) are just higher order harmonics of the template wave vector (SI Figure S7), and should be weak. If the nucleation centers look exactly like the particle (same e-beam contrast, diameter, etc.), the lower order peaks should disappear to achieve spatial frequency multiplication. For $x$ = 2.7d, the particles will align to the other third order $k_t$ vectors, as noted in green in Figure 8g (and noted in the FFT by arrows in SI Figure S7a,b). Smaller x results in a slightly larger magnitude of $k_t$, while the magnitude of $k_p$ to stay the same as for the $3d$ case due to the same particle diameter. As a result, the $k_p$ ($x$ = 2.7d) will align to the other third order peak of the template pattern, which is shorter than that in the $3d$ case. Here, the exact magnitude of $k_t$ can be calculated by basic geometry, using the right triangle formed between the adjacent $k_t$ and $k_y$ vectors. According to this calculation, $k_p = \sqrt{7.6}k_t \sim 2.7k_t$, that is, $x \sim 2.7d$, which matches the experimentally obtained noninteger x for ordered assembly in the first regime. Furthermore, the angle between the two vectors as calculated from the triangle is 19.1°, which precisely matches the angle between the two vectors in the reciprocal pattern (Figure 8h). The same analysis can, of course, be done for templates with larger spacing, for which there are more higher-order wave vectors that the particles can align to the vectors of the template, and the results will be identical to those obtained in the analysis in the space domain.

It should be finally noted, that all the above-described analyses are based on purely geometric considerations. However, the self-assembly described in this work is a kinetic

process, and the presented theoretical analysis does not take into the kinetic fluctuations from the ideally assembled pattern. These fluctuations are produced by randomized local forces, and these forces compete with the directed capillary forces produced by highly ordered nucleation centers. Importantly, the more distant are the nucleation center from each other, the weaker are the capillary forces produce on the assembled nanoparticles, and thus the more dominant the fluctuations become. This explains why the order predicted by the model is more pronounced in the case of nucleation lattice with the low periodicity (i.e., 3d), and gradually reduces as the periodicity decreases. From a practical perspective, it seems from the obtained results that the nucleation patterns with the periodicity of 5d and below are applicable for the fabrication of variably ordered structures, yet the structures obtained from the nucleation lattices with higher periodicity will have a low order, which makes it likely unsuitable for practical applications. However, we must also remember that the periodicity of the nucleation lattice is not the only parameter that affects the order of the assembly, but also the assembly parameters. High control of the environmental conditions, such as humidity that greatly affects the water evaporation and the dynamics of the meniscus drying can probably improve the quality of the assembly.[37] In addition to varying the environmental conditions of kinetically driven assembly, we envisage that modulating the intrinsic nanoparticle properties such as their surface energy and Zeta-potential, that affect particle interactions at the liquid−air interfaces,[38] as well as the materials from which the nanoparticles are made can also have a profound impact on their assembly. This therefore is currently the subject of ongoing research in our laboratory. Applying a highly controlled assembly of nanospheres into a monolayer by the Langmuir−Blodgett method can further improve the order of the obtained structures, and this is the subject of our current study.

## CONCLUSIONS

We presented here a new approach for the assembly of nanoparticles into continuous superlattices controlled by lithographic templates. Here, the templates consisted of guiding features with sizes equal to the assembled nanoparticles and arranged in hexagonal geometry. We showed that these guiding features act as nucleation centers for the 2D structures formed by the assembled nanoparticles and that by slightly varying the spacing between the guiding features, a wide variety of assembly patterns can be obtained. In particular, we showed that for a relatively short-range of spacing, which is in the order of a few diameters of the nanoparticles, four different types of assembled patterns can be obtained, depending on the exact spacing between the nucleation centers, including completely disordered patterns, patterns with simple periodic hexagonal order, and patterns with complex geometries in which nanoparticles are assembled into ordered clusters whose geometry and orientation are controlled by the spacing between the nucleation centers. We introduced a simple geometrical model to analyze the results, which is able to predict for a given nucleation center lattice spacing the number of allowed configurations and their rotations relative to the nanoparticle lattice. From the mathematical analysis of the assembled pattern, it stems that the systems will try to reach closely packed hexagonal assembly whenever the arrangement of the nucleation centers allows this. The spacing between the nucleation centers, in this case,

can either fit the hexagonal assembly lattice or not, and accordingly lead to an ordered or disordered assembly, respectively. In the former case, the orientation of the assembled structure can be controlled solely by the spacing between the nucleation centers.

Besides controlling the orientation of assembly, we demonstrated here the bottom-up fabrication of superlattices with a geometry different from natural self-assembly. Such a fabrication can be applied, for instance, to produce "plasmonic molecules", in which two or more nanoparticles are coupled to produce "hot-spots" of the electric field between them. Up to date, bottom-up fabricated plasmonic molecules were limited to two or three nanoparticles, whereas ordered plasmonic molecules of a higher number of nanoparticles could be produced only from the top-down. The assembly of nanoparticles into separated clusters, as obtained in the fourth assembly regime for nucleation centers separated by the spacing slightly higher than 3d, opens an intriguing route for the scalable fabrication of complex plasmonic molecules by the hybrid top-down/bottom-up approach. Also, the current study explored the effect of only one geometric parameter—the spacing between the nucleation centers—on the assembly of nanoparticles. Naturally, other parameters, such as the size, arrangement, and chemical composition of the nucleation center can be potentially exploited to control the assembly, and together provide a powerful toolbox for the structuring of complex nanoscale architectures. The effect of these parameters on the assembly geometry will be further explored in our follow-up studies. Finally, this study has been limited to periodic lithographic templates. On the other hand, non-periodic templates can be designed to yield nonperiodic assembled patterns with controllably induced defects and disorder, whose emerging applications of include but are not limited to broadband light trapping plasmonics for light-trapping in photovoltaics,[39] as well as broadband antireflective nanostructures.[40,41] In summary, the present findings provide new insight into the templated self-assembly and pave the way to numerous nanoscale systems realized from the bottom-up.

## ASSOCIATED CONTENT

**ⓢ Supporting Information**

The Supporting Information is available free of charge at https://pubs.acs.org/doi/10.1021/acs.langmuir.1c01188.

SEM images and FFTs of assembled nanoparticles on the templated surfaces (PDF)

## AUTHOR INFORMATION

**Corresponding Author**

**Mark Schvartzman** − *Department of Materials Engineering and Ilse Katz Institute for the Nanoscale Science and Technology, Ben-Gurion University of the Negev, Beer-Sheva 84105, Israel;* ⓞ orcid.org/0000-0002-5912-525X; Email: marksc@bgu.ac.il

**Authors**

**Natali Ostrovsky** − *Department of Materials Engineering and Ilse Katz Institute for the Nanoscale Science and Technology, Ben-Gurion University of the Negev, Beer-Sheva 84105, Israel*

**Guillaume Le Saux** − *Department of Materials Engineering and Ilse Katz Institute for the Nanoscale Science and Technology, Ben-Gurion University of the Negev, Beer-Sheva 84105, Israel;* ⓞ orcid.org/0000-0003-4902-1980

**Uri Argaman** − *Department of Materials Engineering, Ben-Gurion University of the Negev, Beer-Sheva 84105, Israel*

**I−Te Chen** − *Walker Department of Mechanical Engineering, The University of Texas, Austin 78712-1139 Texas, United States;* ⊙ orcid.org/0000-0001-5684-290X

**Timothy Chen** − *Department of Mechanical & Aerospace Engineering, North Carolina State University, Raleigh 27695 North Carolina, United States*

**Chih-Hao Chang** − *Walker Department of Mechanical Engineering, The University of Texas, Austin 78712-1139 Texas, United States;* ⊙ orcid.org/0000-0003-4268-4108

**Guy Makov** − *Department of Materials Engineering and Ilse Katz Institute for the Nanoscale Science and Technology, Ben-Gurion University of the Negev, Beer-Sheva 84105, Israel;* ⊙ orcid.org/0000-0003-4145-7245

Complete contact information is available at:
https://pubs.acs.org/10.1021/acs.langmuir.1c01188

**Notes**

## ◼ ACKNOWLEDGMENTS

## ◼ REFERENCES

(1) Alivisatos, A. P. Semiconductor Clusters, Nanocrystals, and Quantum Dots. *Science* **1996**, *272* (5251), 933−937.

(2) Iijima, S.; Ichihashi, T. Single-Shell Carbon Nanotubes of 1-Nm Diameter. *Nature* **1993**, *363*, 603−605.

(3) Tenne, R. Inorganic Nanotubes and Fullerene-like Nano-particles. *Nat. Nanotechnol.* **2006**, *1*, 103−111.

(4) Rothemund, P. W. K. Folding DNA to Create Nanoscale Shapes and Patterns. *Nature* **2006**, *440*, 297−302.

(5) Wu, Y.; Cui, Y.; Huynh, L.; Barrelet, C. J.; Bell, D. C.; Lieber, C. M. Controlled Growth and Structures of Molecular-Scale Silicon Nanowires. *Nano Lett.* **2004**, *4* (3), 433−436.

(6) Whitesides, G. M.; Grzybowski, B. Self-Assembly at All Scales. *Science* **2002**, *295* (5564), 2418−2421.

(7) Gobre, V. V.; Tkatchenko, A. Scaling Laws for van Der Waals Interactions in Nanostructured Materials. *Nat. Commun.* **2013**, *4* (1), 1−6.

(8) Rothemund, P. W. K. Using Lateral Capillary Forces to Compute by Self-Assembly. *Proc. Natl. Acad. Sci. U. S. A.* **2000**, *97* (3), 984−989.

(9) Bowden, N.; Choi, I. S.; Grzybowski, B. A.; Whitesides, G. M. Mesoscale Self-Assembly of Hexagonal Plates Using Lateral Capillary Force: Synthesis Using the "Capillary Bond. *J. Am. Chem. Soc.* **1999**, *121* (23), 5373−5391.

(10) Ni, S.; Leemann, J.; Wolf, H.; Isa, L. Insights into Mechanisms of Capillary Assembly. *Faraday Discuss.* **2015**, *181* (0), 225−242.

(11) Ni, S.; Isa, L.; Wolf, H. Capillary Assembly as a Tool for the Heterogeneous Integration of Micro- and Nanoscale Objects. *Soft Matter* **2018**, *14* (16), 2978−2995.

(12) Van Blaaderen, A.; Ruel, R.; Wiltzius, P. Template-Directed Colloidal Crystallization. *Nature* **1997**, *385* (6614), 321−323.

(13) Flauraud, V.; Mastrangeli, M.; Bernasconi, G. D.; Butet, J.; Alexander, D. T. L.; Shahrabi, E.; Martin, O. J. F.; Brugger, J. Nanoscale Topographical Control of Capillary Assembly of Nano-particles. *Nat. Nanotechnol.* **2017**, *12* (1), 73−80.

(14) Greybush, N. J.; Saboktakin, M.; Ye, X.; Della Giovampaola, C.; Oh, S. J.; Berry, N. E.; Engheta, N.; Murray, C. B.; Kagan, C. R. Plasmon-Enhanced Upconversion Luminescence in Single Nano-phosphor-Nanorod Heterodimers Formed through Template-Assisted Self-Assembly. *ACS Nano* **2014**, *8* (9), 9482−9491.

(15) Dustin, M. L.; Baldari, C. T. The Immune Synapse. *Methods Mol. Biol., Vol 1584*; Humana Press: New York, NY, 2017.

(16) Greybush, N. J.; Pacheco-Pen, V.; Engheta, N.; Murray, C. B.; Kagan, C. R. Plasmonic Optical and Chiroptical Response of Self-Assembled Au Nanorod Equilateral Trimers. *ACS Nano* **2019**, *13*, 1617−1624.

(17) Agrawal, H.; Garnett, E. C. Nanocube Imprint Lithography. *ACS Nano* **2020**, *14* (9), 11009−11016.

(18) Henzie, J.; Andrews, S. C.; Ling, X. Y.; Li, Z.; Yang, P. Oriented Assembly of Polyhedral Plasmonic Nanoparticle Clusters. *Proc. Natl. Acad. Sci. U. S. A.* **2013**, *110* (17), 6640−6645.

(19) Chen, T.; Reinhard, B. M. Assembling Color on the Nanoscale: Multichromatic Switchable Pixels from Plasmonic Atoms and Molecules. *Adv. Mater.* **2016**, *28* (18), 3522−3527.

(20) Fan, J. A.; Bao, K.; Sun, L.; Bao, J.; Manoharan, V. N.; Nordlander, P.; Capasso, F. Plasmonic Mode Engineering with Templated Self-Assembled Nanoclusters. *Nano Lett.* **2012**, *12* (10), 5318−5324.

(21) Lee, J.; Seo, J.; Kim, D.; Shin, S.; Lee, S.; Mahata, C.; Lee, H. S.; Min, B. W.; Lee, T. Capillary Force-Induced Glue-Free Printing of Ag Nanoparticle Arrays for Highly Sensitive SERS Substrates. *ACS Appl. Mater. Interfaces* **2014**, *6* (12), 9053−9060.

(22) Cordeiro, J.; Funfschilling, F.; Lecarme, O.; Dias, G. O.; Picard, E.; Peyrade, D. On-Chip Polychromatic Visible Light Emitters Obtained by 3D Capillary Force Assembly. *Microelectron. Eng.* **2013**, *110*, 414−417.

(23) Cui, Y.; Björk, M. T.; Liddle, J. A.; Sönnichsen, C.; Boussert, B.; Alivisatos, A. P. Integration of Colloidal Nanocrystals into Litho-graphically Patterned Devices. *Nano Lett.* **2004**, *4* (6), 1093−1098.

(24) Kraus, T.; Malaquin, L.; Schmid, H.; Riess, W.; Spencer, N. D.; Wolf, H. Nanoparticle Printing with Single-Particle Resolution. *Nat. Nanotechnol.* **2007**, *2* (9), 570−576.

(25) Chou, Y. C.; Wen, C. Y.; Reuter, M. C.; Su, D.; Stach, E. A.; Ross, F. M. Controlling the Growth of Si/Ge Nanowires and Heterojunctions Using Silver-Gold Alloy Catalysts. *ACS Nano* **2012**, *6* (7), 6407−6415.

(26) Yin, Y.; Lu, Y.; Gates, B.; Xia, Y. Template-Assisted Self-Assembly: A Practical Route to Complex Aggregates of Mono-dispersed Colloids with Well-Defined Sizes, Shapes, and Structures. *J. Am. Chem. Soc.* **2001**, *123* (36), 8718−8729.

(27) Xia, Y.; Yin, Y.; Lu, Y.; McLellan, J. Template-Assisted Self-Assembly of Spherical Colloids into Complex and Controllable Structures. *Adv. Funct. Mater.* **2003**, *13* (12), 907−918.

(28) Koh, K.; Hwang, H.; Park, C.; Lee, J. Y.; Jeon, T. Y.; Kim, S. H.; Kim, J. K.; Jeong, U. Large-Area Accurate Position Registry of Microparticles on Flexible, Stretchable Substrates Using Elastomer Templates. *ACS Appl. Mater. Interfaces* **2016**, *8* (41), 28149−28158.

(29) Elek, J. E.; Zhang, X. A.; Dai, B.; Xu, Z.; Chang, C. H. Fabrication of Three-Dimensional Hierarchical Nanostructures Using Template-Directed Colloidal Assembly. *Nanoscale* **2015**, *7* (10), 4406−4410.

(30) Wang, L.; Dong, L.; Li, L.; Ding, R.; Liu, J.; Zhang, W.; Wang, Y.; Weng, Z.; Guo, X.; Wang, Z. Templated Assembly of Micropatterned Au-Ni Nanoparticles on Laser Interference-Struc-tured Surfaces by Thermal Dewetting. *J. Magn. Magn. Mater.* **2020**, *495*, 165876.

(31) Guo, X.; Li, S.; Lei, Z.; Liu, R.; Li, L.; Wang, L.; Dong, L.; Peng, K.; Wang, Z. Controllable Patterning of Hybrid Silicon Nanowire and Nanohole Arrays by Laser Interference Lithography. *Phys. Status Solidi RRL* **2020**, *14* (6), 2000024.

(32) Von Freymann, G.; Kitaev, V.; Lotschz, B. V.; Ozin, G. A. Bottom-up Assembly of Photonic Crystals †. *Chem. Soc. Rev.* **2528**, *42*, 2528.

(33) Kadiri, H.; Kostcheev, S.; Turover, D.; Salas-Montiel, R.; Nomenyo, K.; Gokarna, A.; Lerondel, G. Topology Assisted Self-Organization of Colloidal Nanoparticles: Application to 2D Large-Scale Nanomastering. *Beilstein J. Nanotechnol.* **2014**, *5* (1), 1203−1209.

(34) Asbahi, M.; Lim, K. T. P.; Wang, F.; Duan, H.; Thiyagarajah, N.; Ng, V.; Yang, J. K. W. Directed Self-Assembly of Densely Packed Gold Nanoparticles. *Langmuir* **2012**, *28* (49), 16782−16787.

(35) Chen, I.; Te; Schappell, E.; Zhang, X.; Chang, C. H. Continuous Roll-to-Roll Patterning of Three-Dimensional Periodic Nanostructures. *Microsystems Nanoeng.* **2020**, *6* (1), 1−11.

(36) Born, M. On the Stability of Crystal Lattices IX. Covariant Theory of Lattice Deformations and the Stability of Some Hexagonal Lattices. *Math. Proc. Cambridge Philos. Soc.* **1942**, *38* (1), 82−99.

(37) Cai, Y.; Zhang Newby, B. Marangoni Flow-Induced Self-Assembly of Hexagonal and Stripelike Nanoparticle Patterns. *J. Am. Chem. Soc.* **2008**, *130*, 6076−6077.

(38) Bigioni, T. P.; Lin, X. M.; Nguyen, T. T.; Corwin, E. I.; Witten, T. A.; Jaeger, H. M. Kinetically Driven Self Assembly of Highly Ordered Nanoparticle Monolayers. *Nat. Mater.* **2006**, *5* (4), 265−270.

(39) Pala, R. A.; Liu, J. S. Q.; Barnard, E. S.; Askarov, D.; Garnett, E. C.; Fan, S.; Brongersma, M. L. Optimization of Non-Periodic Plasmonic Light-Trapping Layers for Thin-Film Solar Cells. *Nat. Commun.* **2013**, *4* (1), 1−7.

(40) Li, X.; He, J.; Liu, W. Broadband Anti-Reflective and Water-Repellent Coatings on Glass Substrates for Self-Cleaning Photovoltaic Cells. *Mater. Res. Bull.* **2013**, *48* (7), 2522−2528.

(41) Han, Z. W.; Wang, Z.; Feng, X. M.; Li, B.; Mu, Z. Z.; Zhang, J. Q.; Niu, S. C.; Ren, L. Q. Antireflective Surface Inspired from Biology: A Review. *Biosurface and Biotribology* **2016**, *2* (4), 137−150.